J. Fluid Mech. (2011), *vol.* 687, *pp.* 584–594.
doi:10.1017/jfm.2011.395

A mechanism for control of turbulent separated flow in rectangular diffusers

Hayder Schneider[1]†, Dominic A. Von Terzi[1,2]‡, Hans-Jörg Bauer[1] and Wolfgang Rodi[3]

[1] Institute for Thermal Turbomachinery, Karlsruhe Institute of Technology, Kaiserstraße 12, 76128 Karlsruhe, Germany

[2] Aeronautics Department, Imperial College London, Prince Consort Road, London SW7 2AZ, UK

[3] Institute for Hydromechanics, Karlsruhe Institute of Technology, Kaiserstraße 12, 76128 Karlsruhe, Germany

(Received 7 June 2011; revised 10 August 2011; accepted 12 September 2011; first published online 18 October 2011)

The turbulent separated flow through an asymmetric diffuser with and without manipulation of incoming turbulence-driven mean secondary vortices (MSVs) from a rectangular duct is investigated by large-eddy simulations. The simulations carried out for two diffuser geometries reveal that by introducing a small amount of mean-flow kinetic energy via the MSVs into the flow, the complex three-dimensional separation behaviour and pressure recovery can be effectively controlled. Manipulated MSVs were found to enhance cross-sectional transport of high-momentum fluid, which determined the location, shape, and size of the separation bubble. The integral effect was a delay or expedition in the onset of separation. This change strongly affected the conversion of mean-flow kinetic energy to pressure, in particular for the front part of the diffuser. In addition, a substantial reduction in total pressure loss could be achieved. The manipulation of the MSVs is an efficient mechanism for performance enhancement in the cases investigated. The results have important implications for both control and statistical modelling of turbulent separated flow in rectangular diffusers.

Key words: flow control, turbulent flows

1. Introduction

A diffuser is a device that decelerates a flow and thereby converts the contained kinetic energy into a useful pressure rise. Diffusers are encountered in a wide range of engineering applications, among which turbomachines for power generation, automobiles and aircraft propulsion constitute important examples. In industrial diffusers with three-dimensional asymmetric geometries and high expansion ratios, the pressure rise is often considerably reduced due to the losses by high turbulence levels, unsteadiness, and flow separation. The reliable and accurate prediction of separated diffuser flows is of great practical interest, but remains a challenge for computational fluid dynamics (CFD).

† Email address for correspondence: hayder.schneider@kit.edu

‡ Current address: GE Global Research, 85748 Garching/Munich, Germany

This was confirmed during two European Research Community on Flow, Turbulence and Combustion (ERCOFTAC) workshops (Jakirlić *et al.* 2011), which aimed at evaluating the predictive capabilities of CFD methods. The test case selected was the separated flow in a three-dimensional asymmetric diffuser for which measurements of two diffuser geometries, hereafter referred to as D1 and D2, were provided by Cherry, Elkins & Eaton (2008). The inflow was the same, namely fully developed turbulent flow in a rectangular duct that displayed secondary motion of Prandtl's second kind. By scrutinizing the workshop results (Jakirlić *et al.* 2011), one can conclude that the quality of the diffuser predictions increased with the capability of the CFD method to represent the mean secondary vortices (MSVs) in the inflow duct.

Schneider *et al.* (2010) demonstrated that Reynolds-averaged Navier–Stokes (RANS) calculations with an eddy-viscosity model yielded qualitatively wrong results. These models cannot reproduce MSVs in the inflow duct. Methods that account for or even resolve these structures generally fare better. In the same study, Schneider *et al.* (2010) performed large-eddy simulation (LES) with near-wall modelling and obtained results that agreed with the experimental data within their accuracy for both D1 and D2. Good results were also reported for D1 employing both wall-resolving LES and a hybrid RANS/LES method (Jakirlić *et al.* 2010). Ohlsson *et al.* (2010) conducted a direct numerical simulation of D1 and observed that streamwise vortices emanating from the corners of the inlet persist into the diffuser. Results from a single simulation were reported and the averaging time was limited due to the large computational cost. As a consequence, the impact of these structures on the mean performance of the diffuser could not be identified, but based on flow visualizations the authors conjectured that the secondary motion governs the separation behaviour. Recent experiments on D1 by Grundmann, Sayles & Eaton (2010) showed that localized spanwise forcing at the diffuser inlet is an effective means for modifying the diffuser performance. This study also demonstrated that there is little sensitivity to the Reynolds number. Experiments with both steady and unsteady forcing along the centreline of one of the expanding walls were performed. For the steady case of interest here, a wall jet towards the corners was produced and the data demonstrated a significantly degraded performance in terms of pressure recovery. A different setup with steady forcing that would provoke flow from the corners to the centreline was not investigated; instead the study focused on promising results with unsteady forcing. From the differences in the streamwise velocity distribution at the inlet, the authors concluded that the forcing generated streamwise vortices. They then proposed that these structures were responsible for the observed change in performance. No data were provided within the diffuser to characterize the streamwise vortices, their modification during forcing, and their effect on the separating flow field and the total pressure loss.

From the literature, we conclude that changes in the secondary flow in the inlet of these three-dimensional diffusers can have a considerable impact on the separating flow field and the diffuser performance, but there are still many open questions. Can steady forcing improve performance or is unsteady forcing needed? How do the manipulated secondary flows impact on the three-dimensional separation behaviour inside the diffuser? What kind of processes lead to a change in pressure recovery? How sensitive are these to geometric changes? Can a significant reduction in total pressure losses be achieved? In particular, the first and last questions are important if one wants to employ passive flow control devices or attempt RANS calculations to design a diffuser with flow control. In order to answer the above questions, we present controlled numerical experiments using LES with and without manipulated

MSVs in the inlet duct for the two geometries D1 and D2. In addition, we assess the implications for both control and statistical modelling of turbulent separated flow in rectangular diffusers.

2. The numerical experiment

2.1. *Computational setup*

The key requirement for the present study was a reliable computational setup. Our approach was to derive a simplified setup that allowed for practical computations which capture the relevant physical mechanisms in the experiments of Cherry *et al.* (2008) and Grundmann *et al.* (2010). The derived setup was largely motivated by the experiments, but included several modifications. The influence of the modifications on the results was extensively examined in the previous studies, that is, during the two ERCOFTAC workshops (Jakirlić *et al.* 2011), and in Schneider *et al.* (2010), von Terzi, Schneider & Fröhlich (2010), von Terzi, Schneider & Bauer (2011) and Schneider *et al.* (2011). These studies included a qualitative and quantitative assessment of the effect of domain extent, grid resolution, averaging time, and the inflow generation method on the LES results. Overall, the computational setup proved to be well suited for the present investigation; it is briefly described in the following.

Figure 1(*a*) presents schematically the computational domains for calculating the flow in the inlet duct (precursor simulation) and in the diffuser and outlet duct (main simulation). The flow is incompressible with a Reynolds number of 10 000, based on the height of the inlet duct, H, and the bulk velocity, U_b. Note that in the following all values are made dimensionless with H and U_b. Instantaneous turbulent inflow data were provided by a precursor simulation running in parallel to the main simulation. The data were generated by enforcing the experimental mass flux and periodicity in the streamwise direction. The inflow of the main simulation was placed one H upstream of the diffuser inlet. The diffuser has a length of 15, and is formed by the continuous expansion of the upper and the right wall of the initially rectangular duct. Two diffuser geometries were considered that have similar expansion ratios, but different aspect ratios. Note that the expansion ratio denotes the outlet-to-inlet area ratio, while the aspect ratio denotes the height-to-width ratio. Figure 1(*b*) illustrates the geometrical properties of the two diffusers D1 and D2. Both diffusers develop from the same rectangular inlet duct with cross-sectional area 1×3.33. At the outlet, the differences in the geometry yield 4×4 for D1, and 3.37×4.51 for D2. This results in an expansion ratio of 4.8 for D1, and 4.56 for D2. The outlet duct had a length of 13. A convective boundary condition was applied in conjunction with a buffer zone at the outlet. No-slip boundary conditions were imposed at the walls.

The incompressible, filtered Navier–Stokes equations were solved using the finite volume flow solver LESOCC2 (Hinterberger 2004). Time advancement was accomplished with a three-step Runge–Kutta method. The spatial discretization was a second-order centred scheme. More details on the numerical method can be found in von Terzi *et al.* (2010). In the LES, the standard Smagorinsky model with $C_s = 0.065$ and van Driest wall-damping was employed as a subgrid-scale (SGS) model. Overall, the contribution of the SGS model was relatively small with a time- and volume-averaged fraction of turbulent to molecular viscosity, ν_t/ν, of the order of $O(10^{-2})$. In contrast to Schneider *et al.* (2010), the present simulations resolve the near-wall region instead of employing a near-wall model. All simulations were performed on the same computational grid with $896 \times 128 \times 192$ cells (22 million). The grid was equidistantly spaced in the streamwise direction and refined towards the walls, such

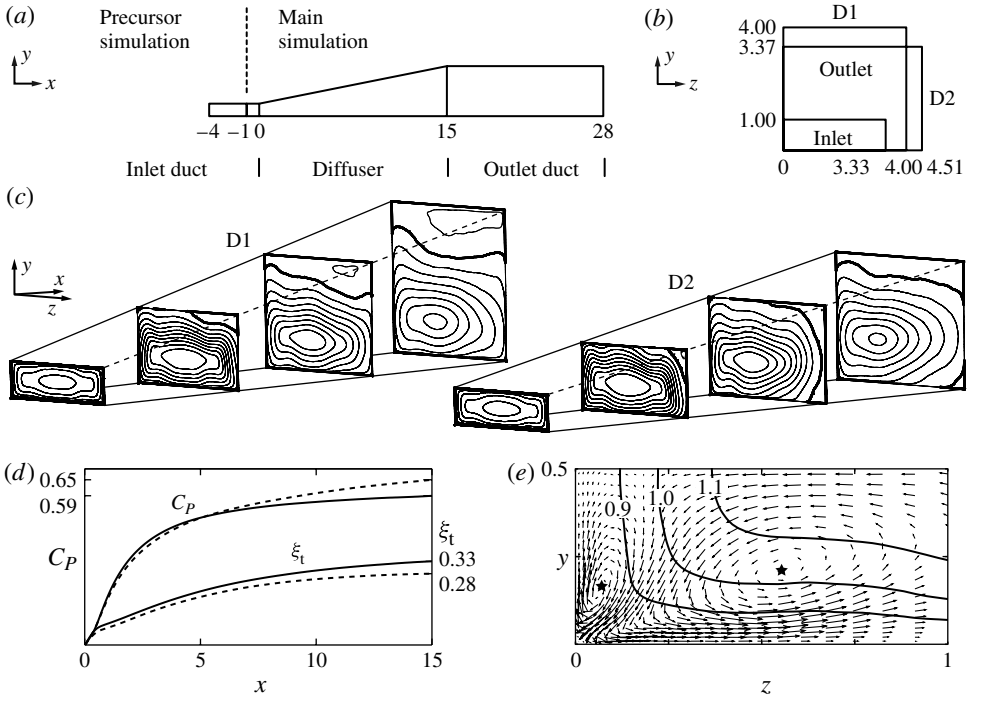

FIGURE 1. (*a*) Computational domain in side view. (*b*) Geometrical properties of D1 and D2 in front view. (*c*) Reference LES in three-dimensional view: contours of mean streamwise velocity, U, with 0.1 intervals shown for cross-sections at $x = 0$, 5, 10, and 15; thicker lines indicate $U = 0$. (*d*) Computed pressure coefficient C_P and total pressure loss coefficient ξ_t, along streamwise coordinate x; ——, D1; - - -, D2. (*e*) Mean secondary flow vectors with superimposed U contours in a corner from precursor simulation; stars indicate centre of rotation; every fourth point shown.

that in the inflow duct $\Delta x^+ = 21$, $1 < \Delta y^+ < 6$, and $1 < \Delta z^+ < 21$. The time step was $4 \times 10^{-3} H/U_b$, and 600 000 time steps were computed. Averaging started after $150H/U_b$, with a total averaging time of $2250H/U_b$.

2.2. *Diffuser assessment*

The characteristics of D1 and D2 are briefly described by inspecting the reference LES. Figure 1(*c*) provides an impression of the geometry and the separated flow fields in the two diffusers. Contours of the mean streamwise velocity, U, with the zero-velocity highlighted, indicate the approximate location, shape and extent of the separation region. In both diffusers the flow separates first at the top right corner; the separation bubble then develops differently due to the different aspect ratio. In D1, the separation extends along the top wall, while in D2, the separation first extends along the top, and then along both the top and the sidewalls. This was shown in Cherry *et al.* (2008) and Schneider *et al.* (2010).

Figure 1(*d*) compares the overall performance of D1 and D2 along the streamwise coordinate x in terms of pressure recovery and total pressure loss. The pressure coefficient is defined as $C_P = (\overline{P} - \overline{P}_{ref})/(1/2\rho U_b^2)$, where the overbar indicates a cross-sectional average, P the mean pressure, and ρ the density. The total pressure loss coefficient is defined as $\xi_t = (\overline{P}_{t,ref} - \overline{P}_t)/\overline{P}_{t,ref}$ where the total pressure is determined

as $\overline{P}_t = \overline{P} - \overline{P}_{ref} + 1/2\rho\overline{U^2}$ in order to compare ξ_t between the diffusers. The reference location was the inlet. It can be seen that D2 performs better than D1, because pressure recovery is higher (+11 %) and total pressure loss is lower (−15 %) at the outlet.

2.3. *Methodology for manipulating secondary flow*

In the experiments of Grundmann *et al.* (2010), plasma actuators upstream of the diffuser inlet were used to introduce low-momentum wall jets that presumably generated streamwise vortices. Since no data on the streamwise vortices or the corresponding three-dimensional velocity-field distribution in the inflow plane is available, the numerical replication of the experimental inflow conditions is associated with a number of uncertainties. Therefore, rather than trying to reproduce the experiments, the focus here is to perform a clean and controlled manipulation of the MSVs in order to fundamentally study their role in the separation behaviour and pressure recovery in the two diffusers.

Figure 1(*e*) shows MSVs in the rectangular inlet duct from the precursor simulation. Recall that these MSVs are of Prandtl's second kind and are turbulence-driven (see Demuren & Rodi 1984, for example). The MSVs are composed of two counter-rotating, elongated and inclined vortices in the corners of the duct. The manipulation of the MSVs is carried out in the entire cross-section at the inflow of the main simulation; it can be summarized as follows:

(*a*) extract instantaneous velocity field, $\boldsymbol{u}$, from the precursor simulation;

(*b*) decompose $\boldsymbol{u}$ into its time-averaged mean, $\boldsymbol{U}$, and its fluctuating part, $\boldsymbol{u}'$;

(*c*) choose a parameter Φ for multiplying the mean secondary velocity components V and W in $\boldsymbol{U} = (U, V, W)^{\mathrm{T}}$;

(*d*) recompose the instantaneous velocity field according to

$$\boldsymbol{u} = (U, \Phi V, \Phi W)^{\mathrm{T}} + \boldsymbol{u}', \tag{2.1}$$

(*e*) introduce the recomposed velocity field as inflow into the main simulation.

It is important to note that the mean streamwise velocity and the turbulent fluctuations are not altered. Therefore, an inflow boundary condition satisfying (2.1) allows us to perform all simulations at the same Reynolds number, mass flux, and inflow time-dependent fluctuations. Hence, the impact of MSVs on the flow field can be studied separately.

Table 1 provides an overview of the three simulations that were performed for both D1 and D2. The baseline (BSL) cases with values of $\Phi = 1$ serve as a reference. In the SVP10 and SVN10 cases, the MSVs were strengthened by a factor of 10 in or against their natural sense of rotation, respectively. Since both secondary components of $\boldsymbol{U}$ are of $O(10^{-2}U_b)$, the overall mean-flow kinetic energy change due to the manipulation is small and of $O(10^{-2}U_b^2)$.

3. Results

3.1. *Secondary flow at inlet*

The application of (2.1) with parameter Φ determined the state of the secondary flow in the inlet duct. This is seen in figure 2(*a*), where MSVs are visualized by contours of the mean streamwise vorticity $\omega_x = \partial W/\partial y - \partial V/\partial z$ at the diffuser inlet. Note that slight asymmetries are due to the starting expansion. For each case, a pair of clockwise (C) and counter-clockwise (CC) rotating vortices is highlighted in the top

Simulation	Modification mode	Φ	Mean-flow energy change
BSL	baseline case (natural state)	1	0
SVP10	steady, strengthened in natural sense of rotation	10	$O(10^{-2}U_b^2)$
SVN10	steady, strengthened against natural sense of rotation	-10	$O(10^{-2}U_b^2)$

TABLE 1. Overview of simulations for D1 and D2: BSL, P, and N denote baseline, positive Φ, and negative Φ, respectively.

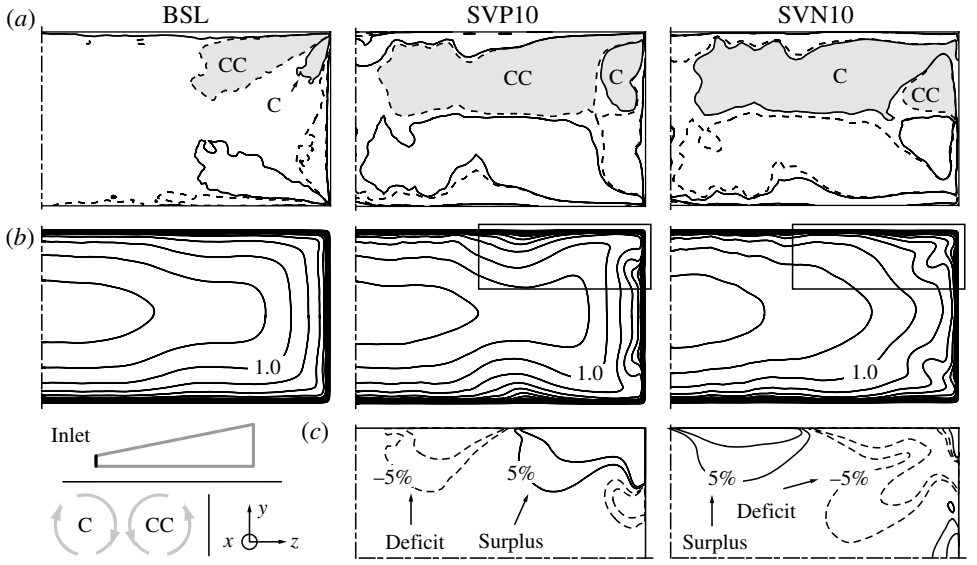

FIGURE 2. Mean flow in right half of diffuser inlet cross-section at $x = 0$. (*a*) $\omega_x = \pm 0.1$ contours; dashed lines are negative levels. (*b*) $0 \leqslant U \leqslant 1.2$ contours with interval 0.1. (*c*) Zoom into regions highlighted by rectangle in (*b*) shows relative deviation of U-velocity with respect to BSL case, $-10\,\% \leqslant \sigma_{rel}(U) \leqslant 10\,\%$ with interval 5 %; dashed lines are negative levels.

right corner. Recall that in the BSL case, the MSVs are of Prandtl's second kind and are turbulence-driven. Comparison with respect to the BSL case shows that the MSVs are significantly strengthened and rotate in or against their natural sense of rotation for cases SVP10 and SVN10, respectively.

The state of the MSVs governs the distribution of the mean streamwise velocity U in the inlet duct. Figure 2(*b*) shows that the manipulation of the MSVs mostly affects the U-velocity distribution in the near-corner regions. In the SVP10 case, the strong MSVs transport more high-momentum fluid from the centre region towards the corners, compared to the BSL case. In the SVN10 case, the opposite is true: low-momentum fluid is transported away from the corners. This is more clearly visualized in figure 2(*c*), where contours of the relative deviation of U with respect to the BSL case, $\sigma_{rel}(U)$, are shown for the near-corner regions highlighted in figure 2(*b*). The manipulation caused either a local surplus (SVP10) or a local deficit (SVN10) of

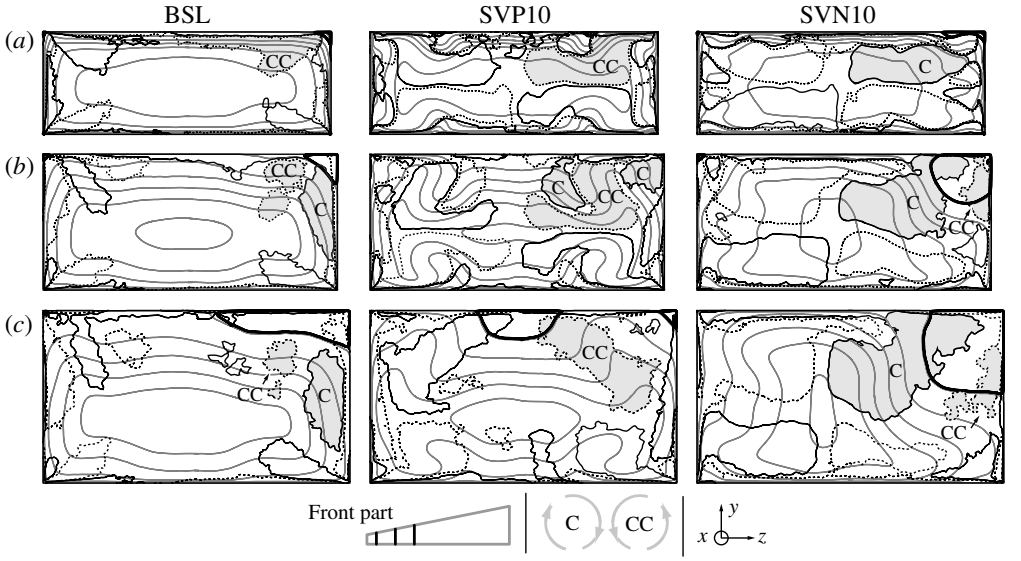

FIGURE 3. The onset of separation in the front part of D1: mean flow in cross-sections at $x = 1$ (*a*), $x = 3$ (*b*), $x = 5$ (*c*); $\omega_x = \pm 0.1$ contours (black dashed lines indicate negative levels) with superimposed $0 \leqslant U \leqslant 1.2$ contours (grey) with interval 0.2; thicker black lines indicate zero-velocity.

high-momentum fluid in the corners. Since the integral of U was kept constant, the MSVs act to redistribute the U-velocity in the cross-section.

3.2. *The onset of separation*

The relative change in the diffuser geometry is particularly strong in two areas: (i) the front part, where the cross-sectional area increases by 100 % until $x = 5$, and (ii) the top right corner of the cross-section, where both walls expand asymmetrically. These geometrical changes determine the onset of separation. Therefore, the focus is on the flow in the top right corner of the front part of the diffuser, and, at first, on D1 only. Figure 3 presents the joint downstream-evolution of the ω_x-vorticity and the U-velocity for streamwise locations with $x \leqslant 5$.

The onset of separation can be seen to depend strongly on the initial mean flow field. In the BSL case, the separation bubble develops in the top right corner, from where it spreads along the top wall to the left. At $x = 5$, there exists both a C- and a smaller CC-structure below the separation bubble. The CC-structure originated from the inlet duct, while the C-structure developed close to the right wall. This constitutes the natural solution; it is in stark contrast to the SVP10 case, in which the separation bubble develops in the centre of the top wall. A close inspection of the CC-structure at $x = 5$ provides a reason for this behaviour. As the artificially strengthened structure evolves into the diffuser, it reorients itself and points to the centre of the top wall. This change seems to be associated with two C-structures emerging between $x = 1$ and 3. These C-structures have disappeared at $x = 5$. However, the remaining CC-structure transports high-momentum fluid from the centre region alongside the right wall via the corner towards the near-corner top wall. A corresponding process occurs in the left half of the cross-section. On the other hand, the CC-structure causes a downward-directed flow in the top centre that transports low-momentum fluid away

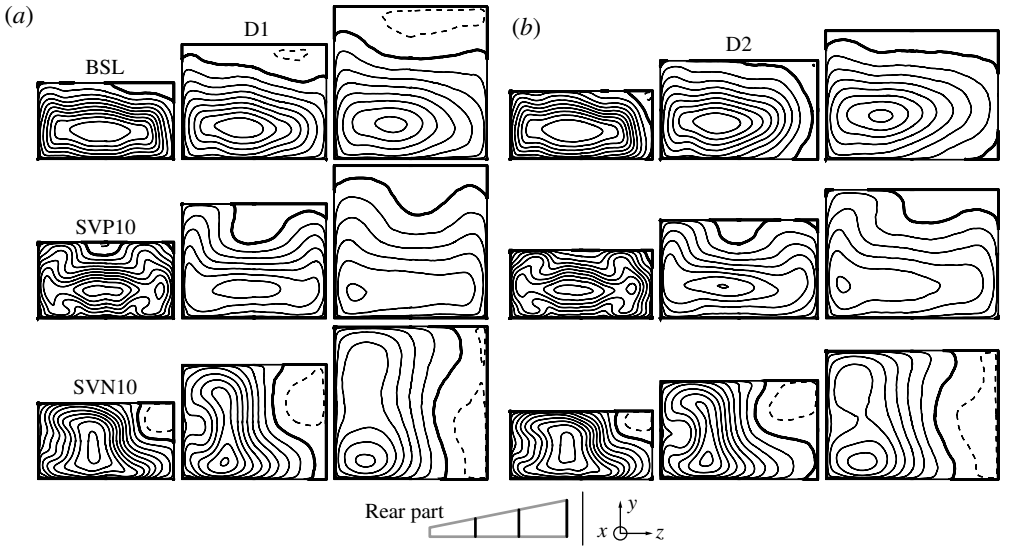

FIGURE 4. Separation and geometric sensitivity in the rear part of D1 (*a*) and D2 (*b*). U contours with interval 0.1 in cross-sections at $x = 5$, 10, and 15 (from left to right); thicker lines indicate zero-velocity; dashed lines are negative values.

from the wall. As in the inlet duct, a local surplus and deficit of high-momentum fluid compared to the BSL case can be observed. The local surplus in the top right corner suppresses the separation, while the local deficit in the centre of the top wall initiates the separation there. The explanation for the SVN10 case is analogous. Strengthening the MSVs, but switching their sense of rotation, enhances the transport of low-velocity fluid away from the top right corner. Compared to the BSL case, the strong C-structure causes a local deficit of high-momentum fluid in this corner and a local surplus in the centre of the top wall. As a result, the separation bubble grows rapidly in the corner and develops alongside the right wall. From the above, it is seen that the enhanced cross-sectional transport of fluid carrying high and low momentum by the MSVs is responsible for the significant differences in the onset of separation.

3.3. *Separation and geometric sensitivity*

The redistributive effect of the MSVs on the U-velocity persists further downstream in the diffuser and proves crucial for the separation behaviour: the initial mean flow field determines the location, shape, and size of the separation bubble. This is shown for both diffusers in figure 4, where the downstream development of the separated flow field is visualized for streamwise locations with $x \geqslant 5$.

By scrutinizing the D1 cases first, distinct qualitative differences can be observed with respect to the reference simulations. In the SVP10 case, the flow separates in the centre of the top wall, then the separation spreads to the right and finally to the left corner of the top wall. The separation bubble undergoes a pronounced undulation in the centre and is altogether smaller than in the BSL case. In the SVN10 case, the flow separates in the top right corner and the separation spreads alongside the right wall to the bottom corner. The separation bubble is entirely shifted toward the right wall and is larger compared to the BSL case. Attention is now turned to D2. While the flow exhibits a strong geometric sensitivity in the BSL cases, this is not observed with manipulated MSVs. For these cases, the separation characteristics of D1 and D2

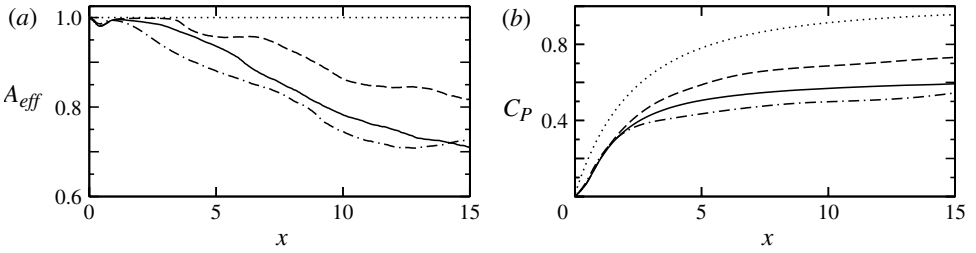

FIGURE 5. Streamwise evolution of separation and pressure recovery for D1: (*a*) effective cross-section A_{eff}; (*b*) pressure coefficient C_P; ——, BSL; - - -, SVP10; – · – · –, SVN10; · · · · · ·, inviscid solution.

bear a strong resemblance to each other. Hence, for both diffusers, the manipulation of the MSVs is an effective means for controlling the separation behaviour and for suppressing the geometric sensitivity of the separation bubble.

3.4. *The influence of separation on pressure recovery*

The integral effect of the MSVs on the separated flow field can be explained by referring back to figures 3 and 4. Depending on whether high-momentum fluid is transported towards or away from the corners, both the onset of separation and the associated downstream growth of the separation bubble is either delayed or expedited, respectively. This is emphasized for D1 by figure 5(*a*), which shows the streamwise evolution of the effective cross-sectional area, A_{eff}, that describes the fractional area occupied by forward flow normalized with the total area. To a first approximation, larger values of A_{eff} indicate a more effective deceleration of the flow and, therefore, an increased conversion of mean-flow kinetic energy to pressure. It is clearly seen that the manipulation delays (SVP10) or expedites (SVN10) the separation growth and hence the effective cross-sectional area.

Figure 5(*b*) shows the streamwise distribution of the pressure coefficient C_P. As a reference for C_P, the ideal solution for the non-separating inviscid case is included as follows from Bernoulli's equation. Compared to the BSL cases, for D1, C_P increased in the SVP10 case by 23 %, and decreased in the SVN10 case by −8 %. Similar pressure variations were achieved for D2: C_P increased by 19 % (SVP10), and decreased by −23 % (SVN10). The same trends can be observed for the total pressure loss coefficient, ξ_t, when compared to the BSL cases. In the SVP10 cases, ξ_t decreased by −31 % (D1) and −35 % (D2), while in the SVN10 cases, ξ_t increased by +15 % (D1) and +42 % (D2). The C_P distribution shows that the largest part of the net pressure rise is due to the pressure gradient history in the first half of the diffuser. This highlights the importance of the onset of separation for the overall pressure recovery: the delay or expedition by the MSVs is the dominant mechanism leading to the significant improvements (SVP10) or degradations (SVN10) in pressure recovery.

4. Conclusions

Controlled numerical experiments were performed to investigate the three-dimensional separation behaviour in an asymmetric diffuser with turbulent inflow from a rectangular duct. Two diffuser geometries were considered. A methodology was presented that allowed for manipulating the turbulence-driven mean secondary vortices in the inlet duct, while keeping the Reynolds number constant and providing time-dependent realistic fluctuations. Applying this methodology, the conjectures in the

literature (Grundmann *et al.* 2010; Ohlsson *et al.* 2010) were confirmed that secondary flows play an important role in the separation dynamics inside the diffuser. Moreover, the underlying physical mechanism was unravelled.

In the absence of manipulation, the separated flow field displayed a pronounced geometric sensitivity. When MSVs at the inlet were manipulated, the geometric sensitivity was suppressed. The results show that both the three-dimensional separation behaviour and the pressure recovery depended on the state of the MSVs. It was found that these structures enhanced cross-sectional transport of streamwise velocity and, as a consequence, determine the location, shape, size, and extent of the separation bubble. For the deliberately chosen manipulation in our setup, the MSVs either enhanced the transport of high-momentum fluid towards the corner or enhanced the transport of low-momentum fluid away from it. The integral effect was to delay or to expedite the onset of separation and the subsequent growth of the separation bubble. It was demonstrated that the largest part of the net pressure rise is due to the pressure gradient history in the first half of the diffuser. A delay in the onset of separation was concomitant with a more effective deceleration of the flow and, thereby, a larger amount of mean-flow kinetic energy was converted to pressure. Despite the small amount of mean-flow kinetic energy input, the pressure recovery was increased or decreased by up to $\pm 23\,\%$ and total pressure losses were changed in a range from $-35\,\%$ to $+42\,\%$ compared to the baseline cases. Hence, the spatial redistribution of high-momentum fluid inside the diffuser through manipulation of MSVs at the diffuser inlet is a potent mechanism for controlling the conversion of mean-flow kinetic energy to pressure, and the diffuser performance.

The results have important implications for both control and statistical modelling of turbulent separated flow in diffusers. (i) The good performance of the steady manipulation suggests that passive flow control devices are indeed an option for future diffuser designs. (ii) The ability to suppress the geometric sensitivity of the flow is of practical importance, since this permits us to change the diffuser design while maintaining a similar flow field and/or pressure rise. (iii) The key importance of the MSVs for the separation requires that statistical turbulence models must adequately account for both the origin of MSVs and their redistributive effect on the streamwise velocity. The results also explain why eddy-viscosity-based RANS models, which inherently cannot account for MSVs, fail in predicting the location and size of the separation bubble. Overall, these findings can help in the development of advanced diffusers with flow control and in the selection and validation of adequate design tools.

Financial support by the German Excellence Initiative and Rolls–Royce Deutschland is gratefully acknowledged. Computer time was provided by the Steinbuch Center for Computing at KIT.

REFERENCES

CHERRY, E. M., ELKINS, C. J. & EATON, J. K. 2008 Geometric sensitivity of three-dimensional separated flows. *Intl J. Heat Fluid Flow* **29** (3), 803–811.

DEMUREN, A. O. & RODI, W. 1984 Calculation of turbulence-driven secondary motion in non-circular ducts. *J. Fluid Mech.* **140**, 189–222.

GRUNDMANN, S., SAYLES, E. & EATON, J. 2010 Sensitivity of an asymmetric 3D diffuser to plasma-actuator induced inlet condition perturbations. *Exp. Fluids* 1–15.

HINTERBERGER, C. 2004 Dreidimensionale und tiefengemittelte Large-Eddy-Simulation von Flachwasserströmungen. PhD thesis, University of Karlsruhe, Karlsruhe, Germany.

JAKIRLIĆ, S., KADAVELIL, G., KORNHAAS, M., SCHÄFER, M., STERNEL, D. C. & TROPEA, C. 2010 Numerical and physical aspects in LES and hybrid LES/RANS of turbulent flow separation in a 3-D diffuser. *Intl J. Heat Fluid Flow* **31** (5), 820–832.

JAKIRLIĆ, S., KADAVELIL, G., SIRBUBALO, S., VON TERZI, D. A., BREUER, M. & BORELLO, D. 2011 14th ERCOFTAC SIG15 Workshop on Refined Turbulence Modelling. *ERCOFTAC Bulletin* **85**.

OHLSSON, J., SCHLATTER, P., FISCHER, P. F. & HENNINGSON, D. S. 2010 Direct numerical simulation of separated flow in a three-dimensional diffuser. *J. Fluid Mech.* **650**, 307–318.

SCHNEIDER, H., VON TERZI, D. A., BAUER, H.-J. & RODI, W. 2010 Reliable and accurate prediction of three-dimensional separation in asymmetric diffusers using Large-Eddy Simulation. *J. Fluids Engng* **132** (3) 031101.

SCHNEIDER, H., VON TERZI, D. A., BAUER, H. -J. & RODI, W. 2011 Impact of secondary vortices on separation dynamics in 3D asymmetric diffusers. In *Direct and Large-Eddy Simulation VIII* (ed. H. Kuerten, B. Geurts, V. Armenio & J. Fröhlich), pp. 443–448. Springer.

VON TERZI, D., SCHNEIDER, H. & BAUER, H.-J. 2011 The impact of secondary mean vortices on turbulent separation in 3D diffusers. In *High Performance Computing in Science and Engineering '10* (ed. W. E. Nagel, D. B. Kröner & M. M. Resch), pp. 339–352. Springer.

VON TERZI, D., SCHNEIDER, H. & FRÖHLICH, J. 2010 Diffusers with three-dimensional separation as test bed for hybrid LES/RANS methods. In *High Performance Computing in Science and Engineering '09* (ed. W. E. Nagel, D. B. Kröner & M. M. Resch), pp. 355–368. Springer.